

# Strongly Enhanced Gilbert Damping in 3d Transition-Metal Ferromagnet Monolayers in Contact with the Topological Insulator Bi<sub>2</sub>Se<sub>3</sub>

Y.S. Hou and R.Q. Wu\*

*Department of Physics and Astronomy, University of California, Irvine, California 92697-4575, USA*

(Received 3 December 2018; revised manuscript received 21 March 2019; published 10 May 2019)

Engineering Gilbert damping of ferromagnetic metal films is of great importance to exploit and design spintronic devices that are operated with an ultrahigh speed. Based on the scattering theory of Gilbert damping, we extend the torque method originally used in studies of magnetocrystalline anisotropy to theoretically determine Gilbert dampings of ferromagnetic metals. This method is utilized to investigate Gilbert dampings of 3d transition-metal ferromagnet iron, cobalt, and nickel monolayers that are contacted by the prototypical topological insulator Bi<sub>2</sub>Se<sub>3</sub>. Amazingly, we find that their Gilbert dampings are strongly enhanced by about one order of magnitude compared with dampings of their bulk forms and free-standing monolayers due to the strong spin-orbit coupling of Bi<sub>2</sub>Se<sub>3</sub>. Our work provides an attractive route for tailoring Gilbert damping of ferromagnetic metallic films by putting them in contact with topological insulators.

DOI: 10.1103/PhysRevApplied.11.054032

## I. INTRODUCTION

In ferromagnets, the time evolution of their magnetization  $\mathbf{M}$  can be described by the Landau-Lifshitz-Gilbert (LLG) equation [1–3]

$$\frac{d\mathbf{M}}{dt} = -\gamma \mathbf{M} \times \mathbf{H}_{\text{eff}} + \frac{\alpha}{M_S} \mathbf{M} \times \frac{d\mathbf{M}}{dt}, \quad (1)$$

where  $\gamma = g\mu_0\mu_B/\hbar$  is the gyromagnetic ratio and  $M_S = |\mathbf{M}|$  is the saturation magnetization. The first term describes the precession motion of magnetization  $\mathbf{M}$  about the effective magnetic field,  $\mathbf{H}_{\text{eff}}$ , which includes contributions from the external field, magnetic anisotropy, exchange, dipole-dipole, and Dzyaloshinskii-Moriya interactions [3]. The second term represents the decay of magnetization precession with a dimensionless parameter  $\alpha$ , known as the Gilbert damping [4–8]. Gilbert damping is known to be important for the performance of various spintronic devices such as hard drives, magnetic random-access memories, spin filters, and magnetic sensors [3,9,10]. For example, Gilbert damping in the free layer of a reader head in a magnetic hard drive determines its response speed and signal-to-noise ratio [11,12]. The bandwidth, insertion loss, and response time of a magnetic thin-film microwave device also critically depend on the value of  $\alpha$  in the film [13].

The rapid development of spintronic technologies calls for the ability of tuning Gilbert damping in a wide range.

Several approaches have been proposed for the engineering of Gilbert damping in ferromagnetic (FM) thin films by using nonmagnetic or rare-earth dopants, adding different seed layers for growth, or adjusting composition ratios in the case of alloy films [9,14–16]. In particular, tuning  $\alpha$  via contact with other materials such as heavy metals, topological insulators (TIs), van der Waals monolayers, or magnetic insulators is promising as the selection of material combinations is essentially unlimited. Some of these materials may have fundamentally different damping mechanisms and offer opportunities for studies of interesting phenomena such as spin-orbit torque, spin-charge conversion, and thermal-spin behavior [17,18].

In this work, we systematically investigate the effect of Bi<sub>2</sub>Se<sub>3</sub> (BS), a prototypical TI, on the Gilbert damping of 3d transition-metal (TM) Fe, Co, and Ni monolayers (MLs) as they are in contact with each other. We find that the Gilbert dampings in the TM-TI combinations are enhanced by about an order of magnitude more than their counterparts in bulk Fe, Co, and Ni as well as in free-standing TM MLs. This drastic enhancement can be attributed to the strong spin-orbit coupling (SOC) of the TI substrate and might also be related to its topological nature. Our work introduces an appealing way to engineer Gilbert dampings of FM metal films by using the peculiar physical properties of TIs.

## II. COMPUTATIONAL DETAILS

Our density-functional theory (DFT) calculations are carried out using the Vienna *Ab initio* Simulation Package (VASP) at the level of the generalized gradient

\*wur@uci.edu

approximation [19–22]. We treat Bi $6s6p$ , Se $4s4p$ , Fe $3d4s$ , Co $3d4s$ , and Ni $3d4s$  as valence electrons and employ the projector-augmented-wave pseudopotentials to describe core-valence interactions [23,24]. The energy cutoff of plane-wave expansion is 450 eV [22]. The BS substrate is simulated by five quintuple layers (QLs), with an in-plane lattice constant of  $a_{\text{BS}} = 4.164$  Å and a vacuum space of 13 Å between slabs along the normal axis. For computational convenience, we put Fe, Co, and Ni MLs on both sides of the BS slab. For the structural optimization of the BS-TM slabs, a  $6 \times 6 \times 1$   $\Gamma$ -centered  $k$ -point grid is used and the positions of all atoms except those of the three central BS QLs are fully relaxed with the criterion that the force on each atom is less than 0.01 eV/Å. The van der Waals (vdW) correction in the form of the nonlocal vdW functional (optB86b-vdW) [25,26] is included in all calculations.

The Gilbert dampings are determined by extending the torque method that we developed for the study of magnetocrystalline anisotropy [27,28]. To ensure numerical convergence, we use very dense  $\Gamma$ -centered  $k$ -point grids and large numbers of unoccupied bands. For example, the first Brillouin zone of BS-Fe is sampled by a  $37 \times 37 \times 1$   $\Gamma$ -centered  $k$  point grid and the number of bands for the second-variation step is set to 396, twice the number (188) of the total valence electrons. More computational details are given in Appendix A. Magnetocrystalline anisotropy energies are determined by computing total energies with different magnetic orientations [29].

### III. TORQUE METHOD OF DETERMINING GILBERT DAMPING

According to the scattering theory of Gilbert damping [30,31], the energy dissipation rate of the electronic system with a Hamiltonian,  $\mathbf{H}(t)$ , is determined by

$$\dot{E}_{\text{dis}} = -\pi\hbar \sum_{ij} \sum_{\mu\nu} \dot{\mathbf{u}}_\mu \dot{\mathbf{u}}_\nu \left\langle \psi_i \left| \frac{\partial \mathbf{H}}{\partial u_\mu} \right| \psi_j \right\rangle \left\langle \psi_j \left| \frac{\partial \mathbf{H}}{\partial u_\nu} \right| \psi_i \right\rangle \times \delta(E_F - E_i) \delta(E_F - E_j). \quad (2)$$

Here,  $E_F$  is the Fermi level and  $\mathbf{u}$  is the deviation of a normalized magnetic moment away from its equilibrium, that is,  $\mathbf{m} = \mathbf{m}_0 + \mathbf{u}$  with  $\mathbf{m}_0 = \mathbf{M}_0/M_s$ . On the other hand, the time derivative of the magnetic energy in the LLG equation is [32]

$$\dot{E}_{\text{mag}} = \mathbf{H}_{\text{eff}} \cdot \frac{d\mathbf{M}}{dt} = \frac{M_s}{\gamma} \sum_{\mu\nu} \alpha_{\mu\nu} \dot{\mathbf{m}}_\mu \dot{\mathbf{m}}_\nu. \quad (3)$$

By taking  $\dot{E}_{\text{dis}} = \dot{E}_{\text{mag}}$ , one obtains the Gilbert damping as

$$\alpha_{\mu\nu} = -\frac{\pi\hbar\gamma}{M_s} \sum_{ij} \left\langle \psi_i \left| \frac{\partial \mathbf{H}}{\partial u_\mu} \right| \psi_j \right\rangle \left\langle \psi_j \left| \frac{\partial \mathbf{H}}{\partial u_\nu} \right| \psi_i \right\rangle \times \delta(E_F - E_i) \delta(E_F - E_j). \quad (4)$$

Note that to obtain Eq. (4), we use  $\partial\mathbf{m} = \partial\mathbf{u}$  since the equilibrium normalized magnetization  $\mathbf{m}_0$  is a constant. In practical numerical calculations,  $\delta(E_F - E)$  is typically substituted by the Lorentzian function  $L(\varepsilon) = 0.5\Gamma/[\pi(\varepsilon - \varepsilon_0)^2 + \pi(0.5\Gamma)^2]$ . The half maximum parameter,  $\Gamma = 1/\tau$ , is adjusted to reflect different scattering rates of electron-hole pairs created by the precession of magnetization  $\mathbf{M}$  [10]. This procedure has been already used in several *ab initio* calculations for Gilbert dampings of metallic systems [8,9,32–35], where the electronic responses play the major role for energy dissipation.

In this work, we focus on the primary Gilbert damping in FM metals that arises from SOC [10,36–38]. There are two important effects in a uniform precession of magnetization  $\mathbf{M}$  when SOC is taken into consideration. The first is the Fermi surface breathing as  $\mathbf{M}$  rotates, that is, some occupied states shift to above the Fermi level and some unoccupied states shift to below the Fermi level. The second is the transition between different states across the Fermi level as the precession can be viewed as a perturbation to the system. These two effects generate electron-hole pairs near the Fermi level and their relaxation through lattice scattering leads to the Gilbert damping.

Now we demonstrate how to obtain the Gilbert damping due to SOC by extending our previous torque method [27]. The general Hamiltonian in Eq. (4) can be replaced by  $\mathbf{H}_{\text{SOC}} = \sum_j \xi(r_j) \mathbf{l}_j \cdot \mathbf{s}$  [4,27] where the index  $j$  refers to atoms, and  $\mathbf{l}_j = -i\mathbf{r}_j \times \nabla$  and  $\mathbf{s}$  are orbital and spin operators, respectively. This is in the same spirit as for the determination of the magnetocrystalline anisotropy [27] for which our torque method is recognized as a powerful tool in the framework of spin-density theory [27]. When  $\mathbf{m}$  points at the direction of  $\mathbf{n}(\theta, \varphi) = (m_x, m_y, m_z)$ , the term  $\mathbf{l} \cdot \mathbf{s}$  in  $\mathbf{H}_{\text{SOC}}$  is written as follows:

$$\begin{aligned} \mathbf{l} \cdot \mathbf{s} = & s_{\mathbf{n}} \left( l_z \cos \theta + \frac{1}{2} l_+ e^{-i\varphi} \sin \theta + \frac{1}{2} l_- e^{i\varphi} \sin \theta \right) \\ & + \frac{1}{2} s_+ \left( -l_z \sin \theta - l_+ e^{-i\varphi} \sin^2 \frac{\theta}{2} + l_- e^{i\varphi} \cos^2 \frac{\theta}{2} \right) \\ & + \frac{1}{2} s_- \left( -l_z \sin \theta + l_+ e^{-i\varphi} \cos^2 \frac{\theta}{2} - l_- e^{i\varphi} \sin^2 \frac{\theta}{2} \right). \end{aligned} \quad (5)$$

To obtain the derivatives of  $\mathbf{H}$  in Eq. (4), we assume that the magnitude of  $\mathbf{M}$  is constant as its direction changes [36]. The processes of getting angular derivatives of  $\mathbf{H}$  are

straightforward and the results are given by Eqs. (B1)–(B5) in Appendix B.

#### IV. RESULTS AND DISCUSSION

In this section, we first show that our approach of determining Gilbert damping works well for FM metals such as 3d TM bulk Fe, Co, and Ni. Following that, we demonstrate the strongly enhanced Gilbert dampings of Fe, Co, and Ni MLs due to contact with BS and then discuss the underlying physical mechanism of these enhancements.

##### A. Gilbert dampings of 3d TM bulk Fe, Co, and Ni

Gilbert dampings of 3d TM bulk bcc Fe, hcp Co, and fcc Ni calculated by means of our extended torque method are consistent with previous theoretical results [10]. As shown in Fig. 1, the intraband contributions decrease whereas the interband contributions increase as the scattering rate  $\Gamma$  increases. The minimum values of  $\alpha$  have the same magnitude as those in Ref. [10] and are comparable

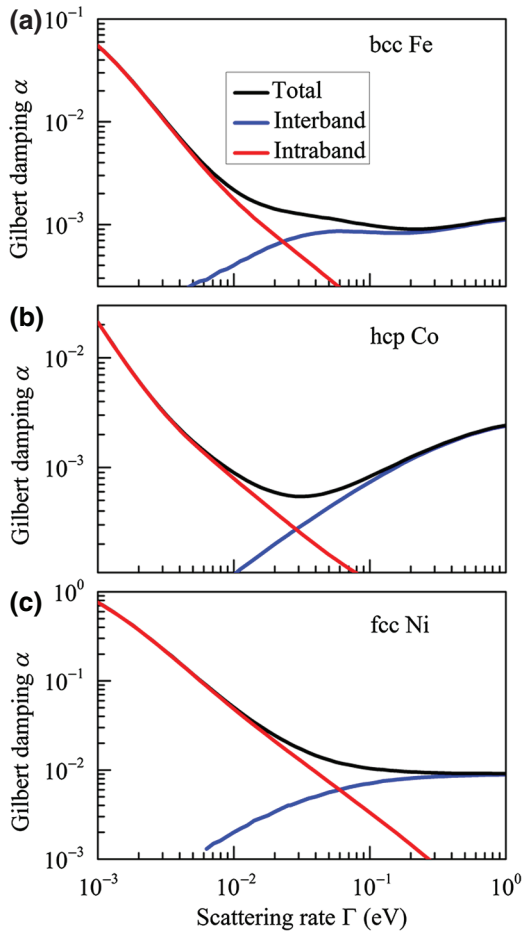


FIG. 1. Gilbert dampings of bulk (a) bcc Fe, (b) hcp Co, and (c) fcc Ni. Black curves give the total Gilbert damping. Red and blue curves give the intraband and interband contributions to the total Gilbert damping, respectively.

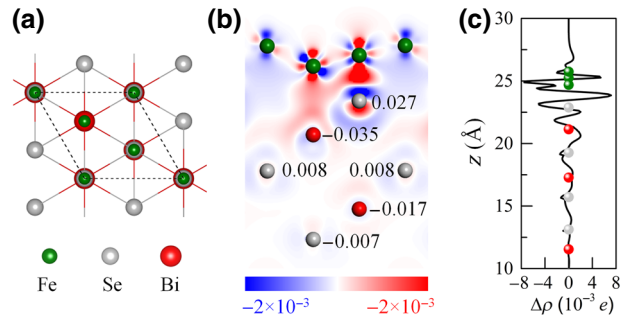


FIG. 2. (a) Top view of atom arrangement in BS-Fe. (b) Charge density difference  $\Delta\rho$  near the interface in BS-Fe. Numbers give the induced magnetic moments (in units of  $\mu_B$ ) in the topmost QL BS. Color bar indicates the weight of negative (blue) and positive (red) charge density differences. (c) Planar-averaged charge density difference  $\Delta\rho$  in BS-Fe. In (a), (b), (c), dark green, light gray, and red balls represent Fe, Se, and Bi atoms, respectively.

with experimentally measured ones [39] for all three metals, showing the applicability of our approach for the determination of Gilbert dampings of FM metals.

##### B. Strongly enhanced Gilbert dampings of Fe, Co, and Ni MLs in contact with BS

We now investigate the magnetic properties of heterostructures of BS and Fe, Co, and Ni MLs. BS-Fe is taken as an example and its atom arrangement is shown in Fig. 2(a). From the spatial distribution of charge density difference  $\Delta\rho = \rho_{BS+Fe-ML} - \rho_{BS} - \rho_{Fe-ML}$  in Fig. 2(b), we see that there is fairly obvious charge transfer between Fe and the topmost Se atoms. By taking the average of  $\Delta\rho$  in the  $xy$ -plane, we find that charge transfer mainly takes place near the interface [Fig. 2(c)]. Furthermore, the charge transfer induces non-negligible magnetization in the topmost QL of BS [Fig. 2(b)]. Similar charge transfers and induced magnetization are also found in BS-Co and BS-Ni (Figs. 6 and Fig. 7 in Appendix C). These suggest that interfacial interactions between BS and 3d TMs are very strong. Note that BS-Fe and BS-Co have in-plane easy axes whereas the BS-Ni has an out-of-plane one.

Figures 3(a) and 3(b) show the  $\Gamma$  dependent Gilbert dampings of BS-Fe, BS-Co and BS-Ni. It is striking that Gilbert dampings of BS-Fe, BS-Co, and BS-Ni are enhanced by about one or two orders of magnitude from the counterparts of bulk Fe, Co, and Ni as well as their free-standing MLs, depending on the choice of scattering rate in the range from 0.001 to 1.0 eV. Similar to bulk Fe, Co, and Ni, the intraband contributions monotonically decrease while the interband contributions increase as the scattering rate  $\Gamma$  gets larger (Fig. 8 in Appendix D). Note that our calculations indicate that there is no obvious difference between the Gilbert dampings of BS-Fe when five and six QL BS slabs are used (Fig. 9 in Appendix E). This is consistent with the experimental observation that the

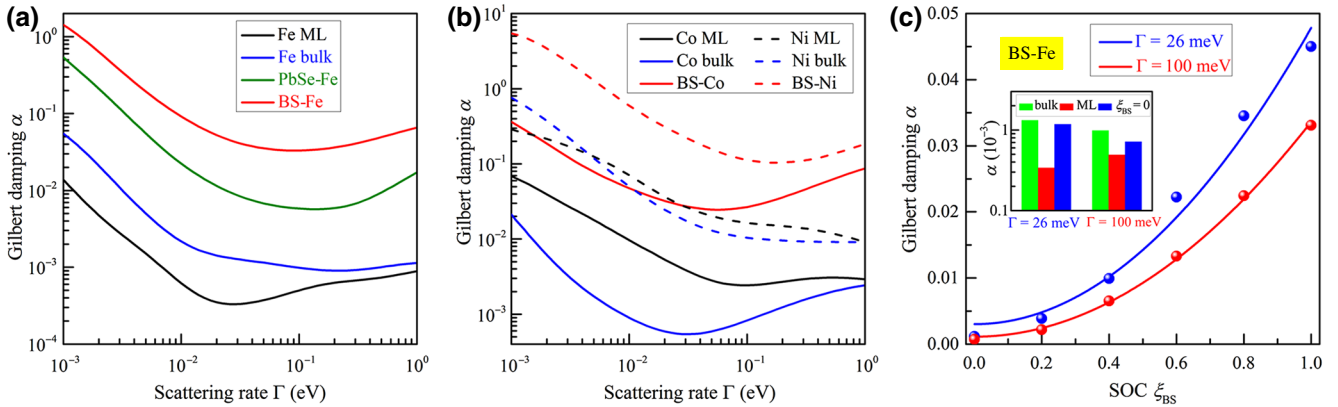


FIG. 3. Scattering rate  $\Gamma$ -dependent Gilbert dampsings of (a) Fe ML, bcc Fe bulk, BS-Fe and PbSe-Fe, (b) Co ML, hcp Co bulk, BS-Co, Ni ML, fcc Ni bulk, and BS-Ni. (c) Dependence of the Gilbert damping of BS-Fe on the scaled SOC  $\xi_{BS}$  of BS in the range from zero ( $\xi_{BS} = 0$ ) to full strength ( $\xi_{BS} = 1$ ). Solid lines show the fitting of Gilbert damping  $\alpha_{BS-Fe}$  to Eq. (6). The inset shows Gilbert damping comparisons between BS-Fe at  $\xi_{BS} = 0$ , bcc Fe bulk, and Fe ML.

interaction between the top and bottom topological surface states is negligible in BS thicker than five QLs [40].

As is well known, TIs are characterized by their strong SOC and topologically nontrivial surface states. An important issue is how they affect the Gilbert dampsings in BS-TM systems. Using BS-Fe as an example, we artificially tune the SOC parameter  $\xi_{BS}$  of BS from zero to full strength and fit the Gilbert damping  $\alpha_{BS-Fe}$  in powers of  $\xi_{BS}$  as

$$\alpha_{BS-Fe} = \alpha_2 \xi_{BS}^2 + \alpha_{BS-Fe}(\xi_{BS} = 0). \quad (6)$$

As shown in Fig. 3(c), we obtain two interesting results: (I) when  $\xi_{BS}$  is zero, the calculated residual Gilbert damping

$\alpha_{BS-Fe}(\xi_{BS} = 0)$  is comparable to Gilbert dampsings of bcc Fe bulk and Fe free-standing ML [see the inset in Fig. 3(c)]; (II) Gilbert damping  $\alpha_{BS-Fe}$  increases almost linearly with  $\xi_{BS}^2$ , similar to previous results [36]. These reveal that the strong SOC of BS is crucial for the enhancement of Gilbert damping.

To gain insight into how the strong SOC of BS affects the damping of BS-Fe, we explore the  $k$ -dependent contributions to Gilbert damping,  $\alpha_{BS-Fe}$ . As shown in Fig. 4(a), many bands near the Fermi level show strong intermixing between Fe and BS orbitals (marked by black arrows). Accordingly, these  $k$  points have large contributions to the Gilbert damping [marked by blue arrows in Fig. 4(b)]. However, if the hybridized states are far away

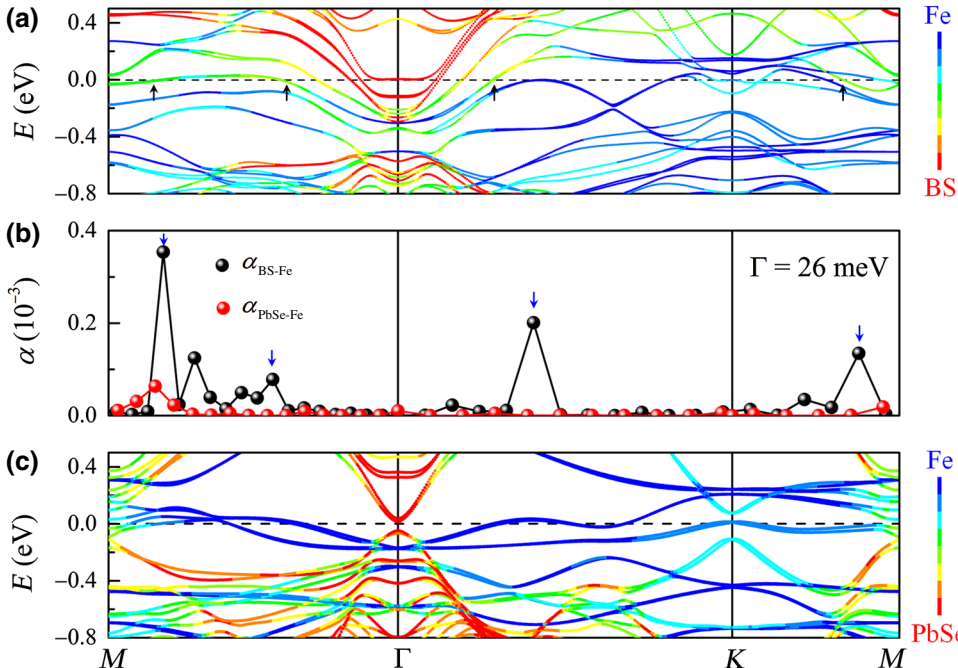


FIG. 4. (a) DFT + SOC calculated band structure of BS-Fe. (b)  $k$  dependent contributions to Gilbert dampsings of BS-Fe (blue dots) and PbSe-Fe (red dots). (c) DFT + SOC calculated band structure of PbSe-Fe. The color bars in (a) and (c) indicate weights of Fe and BS or PbSe. The Fermi level is shown by the black dashed horizontal lines in (a) and (c).

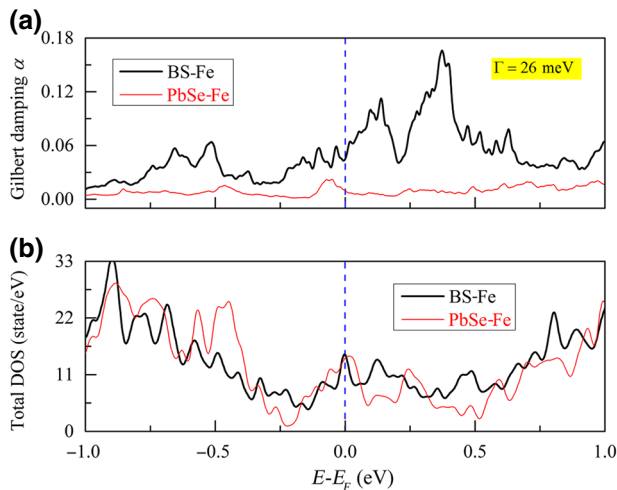


FIG. 5. (a) Gilbert dampings of BS-Fe (black lines) and PbSe-Fe (red line). (b) Total DOS of BS-Fe (black line) and PbSe-Fe (red line). In (a) and (b), the Fermi level  $E_F$  is set to be zero and is indicated by the vertical blue lines.

from the Fermi level, they make almost zero contribution to the Gilbert damping. Therefore, we conclude that only hybridizations at or close to the Fermi level have dominant influence on the Gilbert damping. This is understandable, since energy differences  $E_F - E_i$  and  $E_F - E_j$  are important in the Lorentzian functions in Eq. (4).

It appears that there is no direct link between the topological nature of BS and the strong enhancement of Gilbert damping. The main contributions to Gilbert damping are not from the vicinity around the  $\Gamma$  point, where the topological nature of BS manifests. Besides, BS should undergo a topological phase transition from trivial to topological as its SOC  $\xi_{\text{BS}}$  increases [41]. If the topological nature of BS dictates the enhancement of Gilbert damping, one should expect a kink in the  $\alpha(\xi_{\text{BS}})$  curve at this phase transition point, but this is obviously absent in Fig. 3(c).

To dig deeper into this interesting issue, we replace the topologically nontrivial BS with a topologically trivial insulator PbSe, because the latter has nearly the same SOC as the former. As shown in Fig. 3(a), the Gilbert damping of PbSe-Fe is noticeably smaller than that of BS-Fe, although both are significantly enhanced from the values of  $\alpha$  of Fe bulk and Fe free-standing ML. Taking the similar SOC and interface geometry between BS-Fe and PbSe-Fe (Fig. 10 in Appendix F), the large difference between the Gilbert dampings of BS-Fe and PbSe-Fe suggests that the topological nature of BS may still have an influence on Gilbert damping. By comparing the band structures of BS-Fe and PbSe-Fe [Figs. 4(a) and 4(c)], one observes that PbSe-Fe obviously has less hybridization at or close to the Fermi level as states around  $E_F$  are almost purely from Fe. Accordingly, PbSe-Fe has very small contributions to Gilbert dampings in the entire Brillouin zone, except in the

vicinity around the  $M$  point where two materials hybridize [Fig. 4(b)]. We perceive that the sharp contrast between BS and PbSe on damping of the Fe film stems from the fact that BS has robust metallic topological surface states, but PbSe does not. Even though the Dirac cone of BS is mostly damaged and shifted away from  $E_F$ , the interconnecting tradeoff is the strong interfacial hybridization. Therefore, one may say that the topological tendency of BS still influences the Gilbert damping through the interfacial hybridization.

A previous study of bulk Fe, Co, and Ni suggested a strong correlation between Gilbert damping and total density of states (DOS) around the Fermi level [36]. To determine if this is applicable here, we show the total DOS and Gilbert damping  $\alpha_{\text{BS-Fe}}$  of BS-Fe as a function of the Fermi level based on the rigid band approximation. As shown in Figs. 5(a) and 5(b) (black lines),  $\alpha_{\text{BS-Fe}}$  and the total DOS behave rather differently in most energy regions. Different behaviors between Gilbert damping  $\alpha_{\text{PbSe-Fe}}$  and the total DOS show up in PbSe-Fe as well [see red lines in Figs. 5(a) and 5(b)]. Therefore, we perceive that although the  $\alpha$ -DOS correlation might work for simple systems like bulk Fe, Co, and Ni, it does not hold in heterostructures as the strength of interfacial hybridization strongly alters the effective SOC from band to band.

## V. SUMMARY

In summary, we extend our previous torque method from determining magnetocrystalline anisotropy energies [27,28] to calculating Gilbert damping of FM metals and apply this approach to Fe, Co, and Ni MLs in contact with TI BS. Remarkably, the presence of the TI BS substrate causes order of magnitude enhancements in their Gilbert dampings. Our studies demonstrate that such strong enhancement is mainly due to the strong SOC of the TI BS substrate. The topological nature of BS may also play a role by facilitating the interfacial hybridization and leaving more states around the Fermi level. Although alloying with heavy elements also enhances Gilbert dampings [32], the use of TIs pushes the enhancement into a much wider range. Our work thus establishes an attractive way for tuning the Gilbert damping of FM metallic films, especially in the ultrathin regime.

## ACKNOWLEDGMENTS

We thank Professors A. H. MacDonald and Q. Niu at University of Texas, Austin, for insightful discussions. We also thank Professor M. Z. Wu at Colorado State University and Professor J. Shi at University of California, Riverside, for sharing their experimental data before publication. Work was supported by DOE-BES (Grant No. DE-FG02-05ER46237). Density-functional theory calculations were performed on parallel computers at NERSC supercomputer centers.

## APPENDIX A: DETAILS OF GILBERT DAMPING CALCULATIONS

To compare Gilbert dampings of Fe, Co, and Ni free-standing MLs with BS-Fe, BS-Co, and BS-Ni, we use  $\sqrt{3} \times \sqrt{3}$  supercells containing three atoms and set their lattice constants to 4.164 Å, which is the same as that of the BS substrate. This means that the lattice constant of their primitive unit cell (containing one atom) is fixed at 2.40 Å. The relaxed lattice constants of Fe (2.42 Å), Co (2.35 Å), and Ni (2.36 Å) free-standing MLs are close to this value, as shown in Table I.

TABLE I. Here are details of Gilbert damping calculations of all systems that are studied in this work.  $n_{VE}$  is the abbreviation for the number of valence electrons and  $n_{TB}$  stands for the number of total bands.  $\eta$  is the ratio between  $n_{VE}$  and  $n_{TB}$ , namely,  $\eta = n_{TB}/n_{VE}$ . Note that five QLs of BS are used in calculations for BS-Fe, BS-Co, and BS-Ni.

| Systems | $a$ (Å) | $b$ (Å) | $c$ (Å) | $k$ -point grid          | $n_{VE}$ | $n_{TB}$ | $\eta$ |
|---------|---------|---------|---------|--------------------------|----------|----------|--------|
| Fe bulk | 2.931   | 2.931   | 2.931   | $35 \times 35 \times 35$ | 16       | 36       | 2.25   |
| Co bulk | 2.491   | 2.491   | 4.044   | $37 \times 37 \times 23$ | 18       | 40       | 2.22   |
| Ni bulk | 3.520   | 3.520   | 3.520   | $31 \times 31 \times 31$ | 40       | 80       | 2.00   |
| Fe ML   | 4.164   | 4.164   | —       | $38 \times 38 \times 1$  | 24       | 56       | 2.33   |
| Co ML   | 4.164   | 4.164   | —       | $37 \times 37 \times 1$  | 27       | 64       | 2.37   |
| Ni ML   | 4.164   | 4.164   | —       | $39 \times 39 \times 1$  | 30       | 72       | 2.40   |
| BS-Fe   | 4.164   | 4.164   | —       | $37 \times 37 \times 1$  | 188      | 396      | 2.11   |
| BS-Co   | 4.164   | 4.164   | —       | $37 \times 37 \times 1$  | 194      | 408      | 2.10   |
| BS-Ni   | 4.164   | 4.164   | —       | $37 \times 37 \times 1$  | 200      | 432      | 2.16   |
| PbSe-Fe | 4.265   | 4.265   | —       | $31 \times 31 \times 1$  | 174      | 368      | 2.16   |

## APPENDIX B: DERIVATIVES OF SOC HAMILTONIAN $\mathbf{H}_{SOC}$ WITH RESPECT TO THE SMALL DEVIATION $\mathbf{u}$ OF MAGNETIC MOMENTS

Based on the SOC Hamiltonian  $\mathbf{H}_{SOC}$  in Eq. (5) in the main text, derivatives of the term  $\mathbf{l} \cdot \mathbf{s}$  against the polar angle  $\theta$  and azimuth angle  $\varphi$  are

$$\begin{aligned} \frac{\partial}{\partial \theta} \mathbf{l} \cdot \mathbf{s} &= s_n \left( -l_z \sin \theta + \frac{1}{2} l_+ e^{-i\varphi} \cos \theta + \frac{1}{2} l_- e^{i\varphi} \cos \theta \right) + \frac{1}{2} s_+ \left( -l_z \cos \theta - \frac{1}{2} l_+ e^{-i\varphi} \sin \theta - \frac{1}{2} l_- e^{i\varphi} \sin \theta \right) \\ &\quad + \frac{1}{2} s_- \left( -l_z \cos \theta - \frac{1}{2} l_+ e^{-i\varphi} \sin \theta - \frac{1}{2} l_- e^{i\varphi} \sin \theta \right), \end{aligned} \quad (B1)$$

and

$$\begin{aligned} \frac{\partial}{\partial \varphi} \mathbf{l} \cdot \mathbf{s} &= s_n \left( 0 + (-i) \times \frac{1}{2} l_+ e^{-i\varphi} \sin \theta + (i) \times \frac{1}{2} l_- e^{i\varphi} \sin \theta \right) + \frac{1}{2} s_+ \left( 0 - (-i) \times l_+ e^{-i\varphi} \sin^2 \frac{\theta}{2} + (i) \times l_- e^{i\varphi} \cos^2 \frac{\theta}{2} \right) \\ &\quad + \frac{1}{2} s_- \left( 0 + (-i) \times l_+ e^{-i\varphi} \cos^2 \frac{\theta}{2} - (i) \times l_- e^{i\varphi} \sin^2 \frac{\theta}{2} \right). \end{aligned} \quad (B2)$$

Note that magnetization  $\mathbf{M}$  is assumed to have a constant magnitude when it precesses. When the normalized magnetization  $\mathbf{m}$  points along the direction of  $\mathbf{n}(\theta, \varphi) = (m_x, m_y, m_z)$ , we have:  $m_x = \sin \theta \cos \varphi$ ,  $m_y = \sin \theta \sin \varphi$ , and  $m_z = \cos \theta$ . Taking  $\mathbf{m} = \mathbf{m}_0 + \mathbf{u}$ ,  $\partial \mathbf{m} = \partial \mathbf{u}$ , and the chain rule together, we obtain derivatives of SOC Hamiltonian  $\mathbf{H}_{SOC}$  with respect to the small deviation  $\mathbf{u}$  of magnetic moments as follows:

$$\left. \frac{\partial \mathbf{H}_{SOC}}{\partial u_x} \right|_{\mathbf{M}=\text{const}} = \frac{\partial \mathbf{H}_{SOC}}{\partial \theta} \frac{\partial \theta}{\partial m_x} + \frac{\partial \mathbf{H}_{SOC}}{\partial \varphi} \frac{\partial \varphi}{\partial m_x} = \cos \theta \cos \varphi \frac{\partial \mathbf{H}_{SOC}}{\partial \theta} - \frac{\sin \varphi}{\sin \theta} \frac{\partial \mathbf{H}_{SOC}}{\partial \varphi}, \quad (B3)$$

$$\left. \frac{\partial \mathbf{H}_{SOC}}{\partial u_y} \right|_{\mathbf{M}=\text{const}} = \frac{\partial \mathbf{H}_{SOC}}{\partial \theta} \frac{\partial \theta}{\partial m_y} + \frac{\partial \mathbf{H}_{SOC}}{\partial \varphi} \frac{\partial \varphi}{\partial m_y} = \cos \theta \sin \varphi \frac{\partial \mathbf{H}_{SOC}}{\partial \theta} + \frac{\cos \varphi}{\sin \theta} \frac{\partial \mathbf{H}_{SOC}}{\partial \varphi}, \quad (B4)$$

and

$$\left. \frac{\partial \mathbf{H}_{\text{SOC}}}{\partial u_z} \right|_{\mathbf{M}=\text{const}} = \frac{\partial \mathbf{H}_{\text{SOC}}}{\partial \theta} \frac{\partial \theta}{\partial m_z} + \frac{\partial \mathbf{H}_{\text{SOC}}}{\partial \varphi} \frac{\partial \varphi}{\partial m_z} = -\sin \theta \frac{\partial \mathbf{H}_{\text{SOC}}}{\partial \theta}. \quad (\text{B5})$$

Combining Eq. (5) and Eqs. (B1)–(B5), we can easily obtain the final formulas for derivatives of SOC Hamiltonian  $\mathbf{H}_{\text{SOC}}$  of magnetization  $\mathbf{m}$ .

### APPENDIX C: CHARGE TRANSFERS AND INDUCED MAGNETIC MOMENTS IN BS-Fe, BS-Co, AND BS-Ni

Here, we compare the charge density differences (planar averages in FIG. 6 and more detailed distributions in a vertical plane in Fig. 7) and the induced magnetic moments on Bi and Se atoms (numbers in Fig. 7) at the BS-Fe, BS-Co and BS-Ni interfaces. It appears that they are very similar in these three systems.

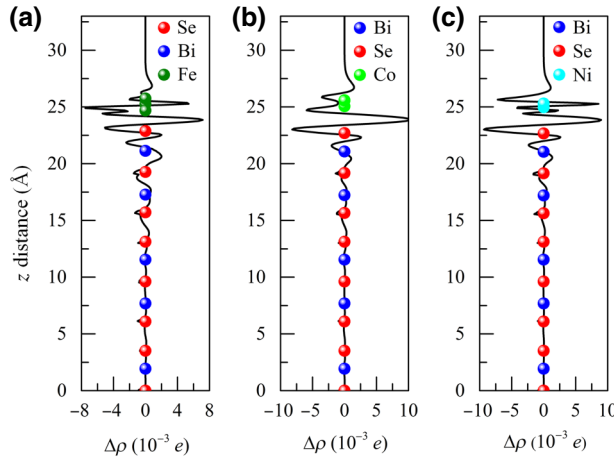


FIG. 6. Planar-averaged charge difference  $\Delta\rho = \rho_{\text{BS+TM-ML}} - \rho_{\text{BS}} - \rho_{\text{TM-ML}}$  (TM = Fe, Co, and Ni) of (a) BS-Fe, (b) BS-Co, and (c) BS-Ni. The atoms' positions are given along the  $z$  axis.

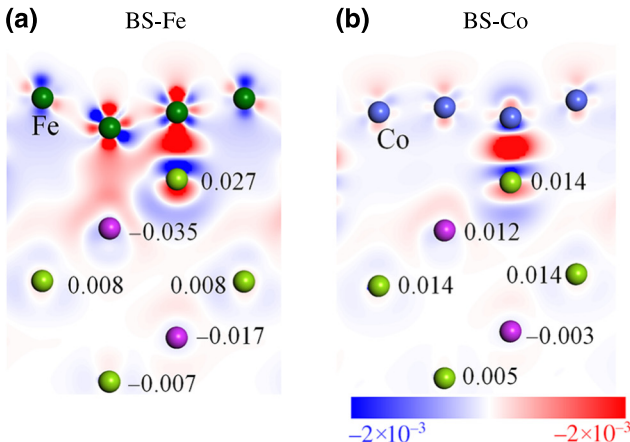


FIG. 7. The redistributions of charge-density difference  $\Delta\rho = \rho_{\text{BS+TM-ML}} - \rho_{\text{BS}} - \rho_{\text{TM-ML}}$  (TM = Fe, Co, and Ni) near the interface between the TM monolayer and the topmost QL BS of (a) BS-Fe, (b) BS-Co, and (c) BS-Ni. The color bar shows the weights of the negative (blue) and positive (red) charge density differences. Numbers give the induced magnetic moments (in units of  $\mu_B$ ) in the topmost QL BS. Bi and Se atoms are shown by the purple and light green balls, respectively.

## APPENDIX D: CONTRIBUTIONS OF INTRABAND AND INTERBAND TO THE GILBERT DAMPINGS OF BS-Fe, BS-Co, AND BS-Ni

By decomposing the total Gilbert dampings of BS-Fe, BS-Co, and BS-Ni into the intraband and interband contributions (FIG. 8), one may observe that the intraband (interband) contributions decrease (increase) monotonically when the scattering rate increases.

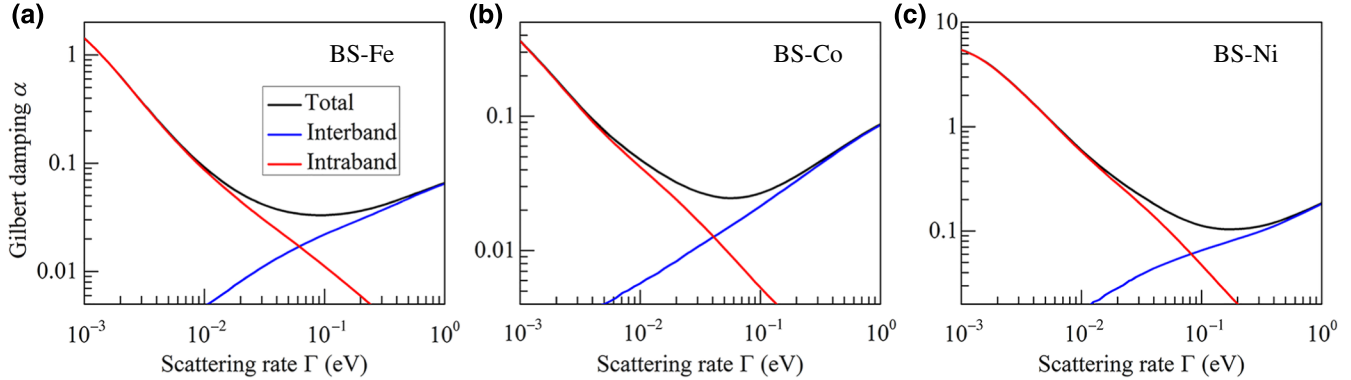


FIG. 8. Calculated Gilbert dampings of (a) BS-Fe, (b) BS-Co, and (c) BS-Ni. Black curves give the total damping. Red and blue curves give the intraband and interband contributions, respectively.

## APPENDIX E: GILBERT DAMPINGS OF BS-Fe WITH FIVE AND SIX QLS OF BS SLABS

Here, we investigate the effect of the thickness of BS slab on the Gilbert dampings of BS-Fe with five and six BS QLs. As shown in FIG. 9, the Gilbert damping appears to be almost unchanged.

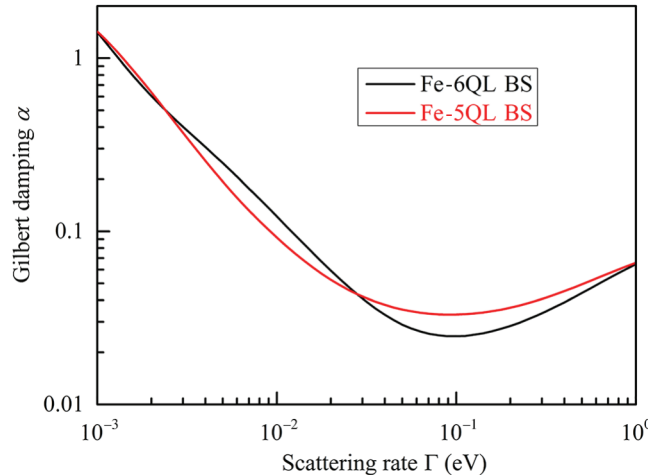


FIG. 9. Gilbert dampings of BS-Fe with five (red) and six (black) QLs of BS slabs. In the calculations of the Gilbert damping of BS-Fe with six QLs of BS, we use a  $39 \times 39 \times 1$  gamma-centered  $k$ -point grid and the number of the total bands is 448, which is twice as large as the number of the total valence electrons (216).

## APPENDIX F: STRUCTURAL COMPARISONS BETWEEN BS-Fe AND PbSe-Fe

To demonstrate the structural similarity between BS-Fe and PbSe-Fe, we show their top and side views and give several Fe-Bi, Fe-Se and Fe-Pb bond lengths in Fig. 10. The main difference between BiSe and PbSe lies on the electronic part as we discussed in the main text.

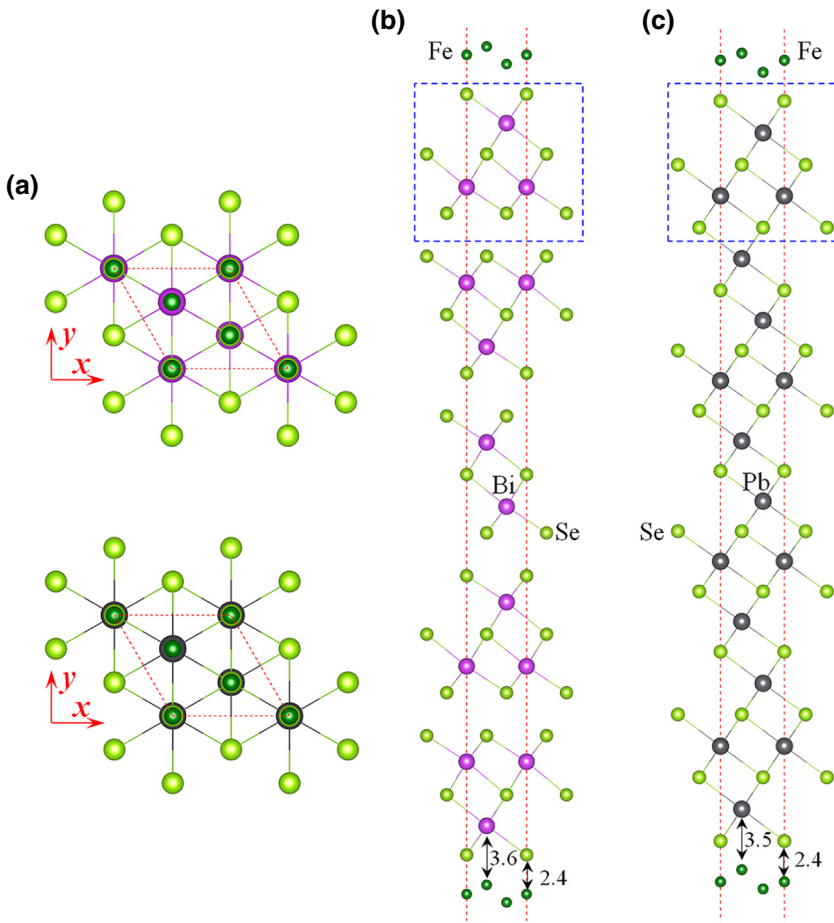


FIG. 10. (a) Top view and (c) side view of atom arrangement in BS-Fe. (b) Top view and (d) side view of atom arrangement in PbSe-Fe. In (a) and (c), the  $xyz$  coordinates are shown by the red arrows. In (b) and (d), the rectangles with blue dashed lines highlight the topmost QL BS in BS-Fe which is similar to the Pb and Se atom layers in PbSe-Fe. The important Fe-Bi, Fe-Se, and Fe-Pb bond lengths are given by the numbers in units of Å. Dark green, light green, purple-red, and dark gray balls represent Fe, Se, Bi, and Pb atoms, respectively. Note that computational details are given in Table I.

- [1] L. Landau and E. Lifshitz, On the theory of the dispersion of magnetic permeability in ferromagnetic bodies, *Phys. Z. Sowjet.* **8**, 101 (1935).
- [2] T. Gilbert, A Lagrangian formulation of the gyromagnetic equation of the magnetization field, *Phys. Rev.* **100**, 1243 (1955).
- [3] T. L. Gilbert, A phenomenological theory of damping in ferromagnetic materials, *IEEE Trans. Magn.* **40**, 3443 (2004).
- [4] D. Steiauf and M. Fähnle, Damping of spin dynamics in nanostructures: an *ab initio* study, *Phys. Rev. B* **72**, 064450 (2005).
- [5] V. L. Safonov, Tensor form of magnetization damping, *J. Appl. Phys.* **91**, 8653 (2002).
- [6] M. Fähnle and D. Steiauf, Breathing Fermi surface model for noncollinear magnetization: A generalization of the Gilbert equation, *Phys. Rev. B* **73**, 184427 (2006).
- [7] D. Thonig and J. Henk, Gilbert damping tensor within the breathing Fermi surface model: anisotropy and non-locality, *New J. Phys.* **16**, 013032 (2014).
- [8] L. Chen, S. Mankovsky, S. Wimmer, M. Schoen, H. Körner, M. Kroneder, D. Schuh, D. Bougeard, H. Ebert, and D. Weiss, Emergence of anisotropic Gilbert damping in ultra-thin Fe layers on GaAs (001), *Nat. Phys.* **14**, 490 (2018).

- [9] M. A. W. Schoen, D. Thonig, M. L. Schneider, T. J. Silva, H. T. Nembach, O. Eriksson, O. Karis, and J. M. Shaw, Ultra-low magnetic damping of a metallic ferromagnet, *Nat. Phys.* **12**, 839 (2016).
- [10] K. Gilmore, Y. Idzerda, and M. Stiles, Identification of the Dominant Precession-Damping Mechanism in Fe, Co, and Ni by First-Principles Calculations, *Phys. Rev. Lett.* **99**, 027204 (2007).
- [11] O. Ertl, G. Hrkac, D. Suess, M. Kirschner, F. Dorfbauer, J. Fidler, and T. Schrefl, Multiscale micromagnetic simulation of giant magnetoresistance read heads, *J. Appl. Phys.* **99**, 08S303 (2006).
- [12] N. Smith, Micromagnetic modeling of magnnoise in magnetoresistive read sensors, *J. Magn. Magn. Mater.* **321**, 531 (2009).
- [13] R. Camley, Z. Celinski, T. Fal, A. Glushchenko, A. Hutchinson, Y. Khivintsev, B. Kuanr, I. Harward, V. Veerakumar, and V. Zagorodnii, High-frequency signal processing using magnetic layered structures, *J. Magn. Magn. Mater.* **321**, 2048 (2009).
- [14] J. Lou, R. Insignares, Z. Cai, K. S. Ziemer, M. Liu, and N. X. Sun, Soft magnetism, magnetostriction, and microwave properties of FeGaB thin films, *Appl. Phys. Lett.* **91**, 182504 (2007).
- [15] L. Lu, J. Young, M. Wu, C. Mathieu, M. Hadley, P. Krivosik, and N. Mo, Tuning of magnetization relaxation

- in ferromagnetic thin films through seed layers, *Appl. Phys. Lett.* **100**, 022403 (2012).
- [16] G. Woltersdorf, M. Kiessling, G. Meyer, J.-U. Thiele, and C. Back, Damping by Slow Relaxing Rare Earth Impurities in Ni<sub>80</sub>Fe<sub>20</sub>, *Phys. Rev. Lett.* **102**, 257602 (2009).
- [17] Y. Tserkovnyak, A. Brataas, and G. E. Bauer, Enhanced Gilbert Damping in Thin Ferromagnetic Films, *Phys. Rev. Lett.* **88**, 117601 (2002).
- [18] Y. Tserkovnyak, A. Brataas, G. E. Bauer, and B. I. Halperin, Nonlocal magnetization dynamics in ferromagnetic heterostructures, *Rev. Mod. Phys.* **77**, 1375 (2005).
- [19] G. Kresse and J. Hafner, *Ab initio* molecular dynamics for liquid metals, *Phys. Rev. B* **47**, 558 (1993).
- [20] G. Kresse and J. Furthmüller, Efficiency of *ab-initio* total energy calculations for metals and semiconductors using a plane-wave basis set, *Comput. Mater. Sci.* **6**, 15 (1996).
- [21] G. Kresse and J. Furthmüller, Efficient iterative schemes for *ab initio* total-energy calculations using a plane-wave basis set, *Phys. Rev. B* **54**, 11169 (1996).
- [22] J. P. Perdew, K. Burke, and M. Ernzerhof, Generalized Gradient Approximation made Simple, *Phys. Rev. Lett.* **77**, 3865 (1996).
- [23] P. E. Blochl, Projector augmented-wave method, *Phys. Rev. B* **50**, 17953 (1994).
- [24] G. Kresse and D. Joubert, From ultrasoft pseudopotentials to the projector augmented-wave method, *Phys. Rev. B* **59**, 1758 (1999).
- [25] J. Klimes, D. R. Bowler, and A. Michaelides, Chemical accuracy for the van der Waals density functional, *J. Phys.: Condens. Matter* **22**, 022201 (2010).
- [26] J. Klimeš, D. R. Bowler, and A. Michaelides, Van der Waals density functionals applied to solids, *Phys. Rev. B* **83**, 195131 (2011).
- [27] X. Wang, R. Wu, D.-S. Wang, and A. J. Freeman, Torque method for the theoretical determination of magnetocrystalline anisotropy, *Phys. Rev. B* **54**, 61 (1996).
- [28] J. Hu and R. Wu, Control of the Magnetism and Magnetic Anisotropy of a Single-Molecule Magnet with an Electric Field, *Phys. Rev. Lett.* **110**, 097202 (2013).
- [29] F. Hajheidari, W. Zhang, and R. Mazzarello, Effects of a magnetic Fe monolayer on the structural and surface electronic properties of Sb<sub>2</sub>Te<sub>3</sub>, *Phys. Rev. B* **94**, 125421 (2016).
- [30] A. Brataas, Y. Tserkovnyak, and G. E. Bauer, Scattering Theory of Gilbert Damping, *Phys. Rev. Lett.* **101**, 037207 (2008).
- [31] A. Brataas, Y. Tserkovnyak, and G. E. Bauer, Magnetization dissipation in ferromagnets from scattering theory, *Phys. Rev. B* **84**, 054416 (2011).
- [32] S. Mankovsky, D. Ködderitzsch, G. Woltersdorf, and H. Ebert, First-principles calculation of the Gilbert damping parameter via the linear response formalism with application to magnetic transition metals and alloys, *Phys. Rev. B* **87**, 014430 (2013).
- [33] A. A. Starikov, P. J. Kelly, A. Brataas, Y. Tserkovnyak, and G. E. Bauer, Unified First-Principles Study of Gilbert Damping, Spin-Flip Diffusion, and Resistivity in Transition Metal Alloys, *Phys. Rev. Lett.* **105**, 236601 (2010).
- [34] H. Ebert, S. Mankovsky, D. Koedderitzsch, and P. J. Kelly, Ab Initio Calculation of the Gilbert Damping Parameter via the Linear Response Formalism, *Phys. Rev. Lett.* **107**, 066603 (2011).
- [35] Y. Liu, Z. Yuan, R. J. Wesselink, A. A. Starikov, and P. J. Kelly, Interface Enhancement of Gilbert Damping from First Principles, *Phys. Rev. Lett.* **113**, 207202 (2014).
- [36] K. Gilmore, Y. U. Idzerda, and M. D. Stiles, Spin-orbit precession damping in transition metal ferromagnets, *J. Appl. Phys.* **103**, 07D303 (2008).
- [37] V. Kamberský, Spin-orbital Gilbert damping in common magnetic metals, *Phys. Rev. B* **76**, 134416 (2007).
- [38] V. Kamberský, On ferromagnetic resonance damping in metals, *Czech. J. Phys. B* **26**, 1366 (1976).
- [39] S. Bhagat and P. Lubitz, Temperature variation of ferromagnetic relaxation in the 3d transition metals, *Phys. Rev. B* **10**, 179 (1974).
- [40] Y. Zhang, K. He, C.-Z. Chang, C.-L. Song, L.-L. Wang, X. Chen, J.-F. Jia, Z. Fang, X. Dai, W.-Y. Shan, S.-Q. Shen, Q. Niu, X.-L. Qi, S.-C. Zhang, X.-C. Ma, and Q.-K. Xue, Crossover of the three-dimensional topological insulator Bi<sub>2</sub>Se<sub>3</sub> to the two-dimensional limit, *Nat. Phys.* **6**, 584 (2010).
- [41] H. Zhang, C.-X. Liu, X.-L. Qi, X. Dai, Z. Fang, and S.-C. Zhang, Topological insulators in Bi<sub>2</sub>Se<sub>3</sub>, Bi<sub>2</sub>Te<sub>3</sub> and Sb<sub>2</sub>Te<sub>3</sub> with a single Dirac cone on the surface, *Nat. Phys.* **5**, 438 (2009).